

Article

Preparation and Properties of Modified Phenylethynyl Terminated Polyimide with Neodymium Oxide

Peng Zhang ^{1,2}, Hansong Liu ², Yilun Yao ², Tao Yang ², Jinsong Sun ², Xiangyu Zhong ², Jianwen Bao ^{2,*}, Yan Zhao ^{1,*} and Xiangbao Chen ^{1,3,*}

¹ School of Materials Science and Engineering, Beihang University, Beijing 100191, China; 050131zhangpeng@163.com

² AVIC Composite Technology Center, AVIC Composite Corporation Ltd., Beijing 101300, China; liuhansong@foxmail.com (H.L.); m2uyao@sina.com (Y.Y.); ytburning@163.com (T.Y.); sunjsbuaa@163.com (J.S.); xyzhong2003@sohu.com (X.Z.)

³ Science and Technology on Advanced Composites Laboratory, Beijing Institute of Aeronautical Materials, Beijing 100095, China

* Correspondence: baojianwen@sohu.com (J.B.); jennyzyhaoyan@buaa.edu.cn (Y.Z.); vcd4321@sina.com (X.C.); Tel.: +86-13693594304 (J.B.)

Abstract: Modified phenylethynyl terminated polyimides (PIs) were successfully prepared by using neodymium oxide (Nd₂O₃) via high-speed stirring and ultrasonic dispersion methods. In addition, the structure and properties of the Nd₂O₃-modified imide oligomers as well as the thermo-oxidative stability of the modified polyimides (PI/Nd₂O₃ hybrid) and its modification mechanism were investigated in detail. The thermogravimetric analysis (TGA) results indicated that the 5% decomposition temperature (Td5%) of the PI/Nd₂O₃ hybrids improved from 557 °C to 575 °C, which was also verified by the TGA-IR tests. Meanwhile, the weight loss rate of the PI/Nd₂O₃ hybrids significantly decreased by 28% to 31% compared to that of pure PI under isothermal aging at 350 °C for 450 h when the added content of Nd₂O₃ was between 0.4 wt% and 1 wt%, showing outstanding thermo-oxidative stability. Moreover, the mechanism of the enhanced thermo-oxidative stability for the modified PIs was analyzed by scanning electron microscopy (SEM) and X-ray diffraction (XRD).

Keywords: phenylethynyl; thermoset polyimide; neodymium oxide; modification; thermo-oxidative stability



Citation: Zhang, P.; Liu, H.; Yao, Y.; Yang, T.; Sun, J.; Zhong, X.; Bao, J.; Zhao, Y.; Chen, X. Preparation and Properties of Modified Phenylethynyl Terminated Polyimide with Neodymium Oxide. *Materials* **2022**, *15*, 4148. <https://doi.org/10.3390/ma15124148>

Received: 25 April 2022

Accepted: 7 June 2022

Published: 10 June 2022

Publisher's Note: MDPI stays neutral with regard to jurisdictional claims in published maps and institutional affiliations.



Copyright: © 2022 by the authors. Licensee MDPI, Basel, Switzerland. This article is an open access article distributed under the terms and conditions of the Creative Commons Attribution (CC BY) license (<https://creativecommons.org/licenses/by/4.0/>).

1. Introduction

Demand for aerospace technology has grown significantly nowadays due to its rapid development, and it now requires materials with better thermo-oxidative stability. Among the various kinds of polymer materials, polyimide (PI) resin and PI matrix composites possess not only outstanding comprehensive properties at high temperatures (280–400 °C), but also the ability to act as load-carrying structures in high temperature environments. In recent years, they have been widely used in aviation, aerospace, and space technology, especially in aero-engines and space aircraft [1–4].

To improve the thermal-oxidation stability of PIs, one conventional method involves finding changes in the chemical characteristics of PI cross-linked structures. For thermosetting PIs, different types of active terminal groups including nadic anhydride-terminated PIs and phenylethynyl-terminated PIs [5–17] can provide the specifics of the resin. The thermal decomposition temperature of nadic anhydride-terminated PIs are generally not higher than 510 °C such as PMR-15, PMR-II-50, RP-46, DMBZ-15, etc. [18–20]. Compared to the former, phenylethynyl-terminated PIs exhibit better thermo-oxidative stability and process performance, which has always been the research focus in this field. Currently, a new generation of PIs has been developed on this basis [8–13] such as PETI-330, PETI-375, AFRPE-4, TriA-X, etc., whose decomposition temperatures are usually between 520 and

550 °C [21–24]. However, to further improve the thermal-oxidation stability over a long period of time by optimizing the chemical structure [14–17], a single pathway by chemical modification has been difficult to achieve the requirements of this performance.

To solve this problem, another way of thinking involves physical modification methods, which have also been proposed. Among these methods, various types of inorganic particles have been used (e.g., graphene oxide, aluminum oxide) for the modification of PIs, which play an important role in improving heat resistance [25–28]. However, the limitation of this method is that many types of particles have a small change in enhancing the thermal performances of the matrix.

Rare earth oxides exhibit outstanding environmental stability [29]. A series of research articles in this field have illustrated that rare earth oxides have a positive effect on the thermal-oxidative stability of polymers such as polyethylene, polyaniline, and thermoplastic PIs. The key sources of the contributing factors of these rare earth oxides involve their distinctive morphologies and catalytic properties [30–36]. Considering the special atomic structural characteristics of rare earth elements, blending PIs with rare earth oxides is a promising method for developing new organic–inorganic hybrid materials as they may combine the properties of inorganics such as heat resistance with the inherent characteristics of PIs.

Many studies have made advances in the field of rare earth oxides [29–44]. A typical example involves using them as thermal stabilizers to enhance the thermal stability of polymers [37–39]. For the modification of thermoset PIs, most studies have reported on enhancing the tribological properties, thermal conductivity as well as gamma-ray/neutron shielding characteristics using rare earth oxides [40,41]. Nevertheless, when it comes to enhancing the thermal stability of thermoset PIs, there have been a small number of relevant articles that can be searched. The influence of choosing proper rare earth oxides as stabilizers for PIs is significant, as the variety of rare earth oxides is numerous and their properties are quite different. Among all the types of rare earth oxides, light rare earth oxides including praseodymium oxide (Pr_6O_{11}), lanthanum oxide (La_2O_3), and neodymium oxide (Nd_2O_3) have the potential to be used for polymer modification. Furthermore, studies [42–46] have shown that Nd_2O_3 has an obvious effect on the polymer's thermal stability.

In our previous research, which was inspired by review studies, a low viscosity type of thermoset PIs and composites were modified with Nd_2O_3 to improve their thermal oxidation stability [47]. The results showed that the weight loss rates of the modified PI composites dramatically decreased by 25% compared to that of the pure PI composites below 350 °C, after aging for 200 h, when the added content of Nd_2O_3 was 1 wt%. However, studies on the influence of the Nd_2O_3 weight content on the thermal-oxidation stability are very limited (only 1%, 3%, and 5 wt%), and it could not be ruled out that the most suitable Nd_2O_3 content may be below 1 wt%. However, we found that Nd_2O_3 could not be uniformly dispersed using the method of high-speed shear dispersion alone, which weakened the thermal oxidation stability. Consequently, in this study, we attempted to use high viscosity PI, combined with high-speed stirring and ultrasonic dispersion methods, to further optimize the amount of Nd_2O_3 and obtain better thermal-oxidation stability.

2. Materials and Methods

2.1. Materials

In this work, the main monomers used for the synthesis of polyimide resin including 2,2'-bis(trifluoromethyl)benzidine (TFMBZ, 99.95%), 2,3,3,4-biphenyltetracarboxylic dianhydride (α -BPDA, 99.95%), and 4-phenylethynylphthalic anhydride (PEPA, 99.95%) were purchased from Changzhou Sunlight Pharmaceutical Co., Ltd., Changzhou, China, and ethanol (AR) was brought from Beijing Chemical Works, Beijing, China. The scanning electron microscope (SEM) pattern of the neodymium oxide (Nd_2O_3 , Sinopharm Chemical Reagent Co., Ltd., Beijing, China) particles is shown in Figure 1.

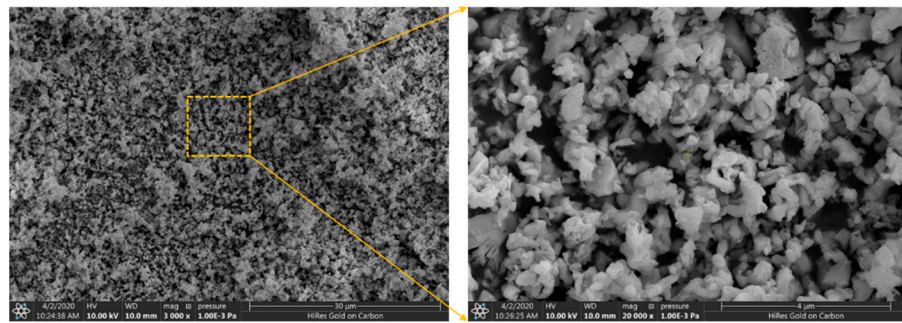


Figure 1. The scanning electron microscope image of Nd_2O_3 .

2.2. Preparation of Nd_2O_3 Modified Polyimide Resin

The PEPA (236.82 g), α -BPDA (280.69 g), and ethyl alcohol (1207.00 g) were first placed in a 2 L beaker and stirred using a glass bar to form a mixed slurry. The slurry was added to a 3 L three-necked flask that was equipped with a mechanical stirrer, reflux condenser, mercury thermometer, and nitrogen gas inlet. Then, the mixture was heated to reflux ($\sim 78^\circ\text{C}$) for approximately 1 h to dissolve the anhydrides, followed by an additional 2 h to complete esterification. Then, the TFMBZ (183.32 g) and another diamine (299.18 g) powder were added, and the solution of amide ester oligomers was obtained after stirring and heating from 78°C to 110°C for ~ 2 h. Afterward, the Nd_2O_3 powder was added according to the addition ratio (0.2, 0.4, 0.6, 0.8, and 1 wt%), under high-speed stirring at 2000–5000 rpm. Subsequently, the mixture was further dispersed by an ultrasonic disperser to obtain better dispersion, and the Nd_2O_3 modified amide ester oligomer was heated up around $150\sim 260^\circ\text{C}$ to complete imidization. After being converted into an imide oligomer, it was then cured at $385 \pm 5^\circ\text{C}$ for 5 h and formed a modified $\text{Nd}_2\text{O}_3/\text{PI}$ hybrid. The synthesis process of the $\text{Nd}_2\text{O}_3/\text{PI}$ hybrid is illustrated in Figure 2.

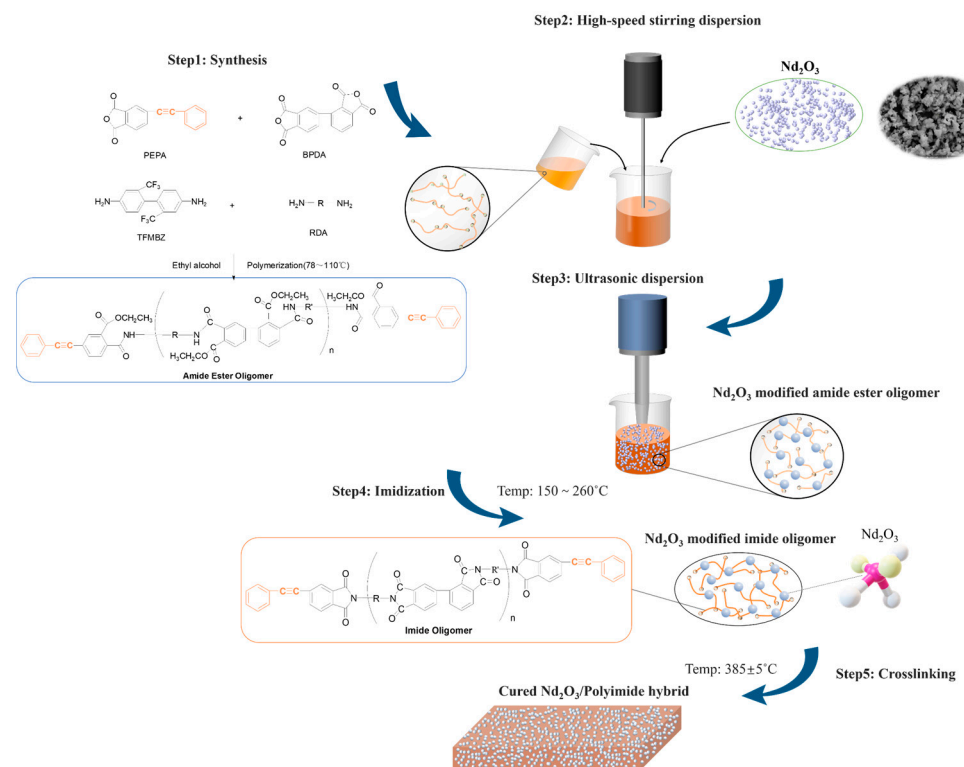


Figure 2. Schematic drawing of the preparation process of the modified polyimide.

2.3. Characterization

The Fourier transform infrared (FTIR) spectra of the modified imide oligomers and Nd₂O₃/PI hybrids with different content Nd₂O₃ were recorded using a Nicolet S50 FTIR spectrophotometer. The X-ray diffraction (XRD) patterns of the Nd₂O₃ modified imide oligomer with varied Nd₂O₃ content as well as unmodified PI and Nd₂O₃/PI hybrids were recorded using a Bruker D8 advance diffractometer (Germany). The diffractogram was measured at an operating 2θ range of 2θ = 3–60°. A SEM was used to investigate the sample shape characteristics using a field emission SEM (FE-SEM, Hitachi S-4800), and a rheology test was used to study the rheological properties of the pure imide oligomer and Nd₂O₃-modified imide oligomers using a TA Instruments AR 2000 rheometer. The oligomer powders were pressed into thin wafers, 2.5 cm in diameter, and tested at a heating rate of 2 °C/min from 260 °C to 400 °C. The glass transition temperature (T_g) of PIs was measured through dynamic mechanical thermal analysis (DMA) using a TA Instruments DMAQ800 dynamic mechanical analyzer from room temperature (RT) to 500 °C at a heating rate of 5 °C/min, under a frequency of 1 Hz, and using the double cantilever deformation mode. Thermogravimetric analysis (TGA) was performed with a NETZSCH STA 449F5 at a heating rate of 10 °C/min from 40 to 800 °C under air purging. The TGA-FTIR studies were carried out using a NETZSCH STA 449F5 thermogravimetric analyzer that was interfaced with a TENSORII FT-IR spectrometer. Thermal oxygen aging was processed in a high temperature forced air oven, and the Nd₂O₃/PI hybrids and pure PI samples were cut into a size of 80 mm × 30 mm × 4 mm. First, the samples were heated to 200 °C and held for 1 h to remove the moisture. Then, the sample weights (recorded as M₀) were recorded by an analytical balance, with a precision of 0.001 g. After that, the samples were placed back into the oven and heated to 350 °C and aged for 450 h. The samples were removed at different times for weighing and recorded as M_t. Accordingly, the weight loss rate at time t was calculated as follows:

$$\Delta M_t = (M_0 - M_t) / M_0 \times 100\%.$$

3. Results and Discussion

3.1. Structure Characterization of Nd₂O₃ Modified Imide Oligomer

The FTIR spectroscopy experiments were performed to investigate whether Nd₂O₃ was successfully added into the imide oligomer and the interactions between them (Figure 3). The characteristic absorption bands related to the pure imide oligomer showed obvious absorption peaks arising from the asymmetric and symmetric stretching vibrations of the C=O groups in the imide rings at around 1779 and 1722 cm⁻¹. Another characteristic absorption band of the imide group derived from C–N stretching appeared at approximately 1369 and 738 cm⁻¹. In addition, the band at 2212 cm⁻¹ was related to the stretching vibrations of the phenylethynyl group (C≡C). Thus, the results indicated that the imide oligomer formed through thermal imidization. The 0.2, 0.4, 0.6, 0.8, and 1 wt% Nd₂O₃ content modified oligomers (Nd₂O₃/oligomer) showed a relatively weak absorption peak at 3605 cm⁻¹, which corresponded well to the O–H of Nd(OH)₃, and we preliminarily inferred that the Nd₂O₃ present in the oligomers was in the form of Nd(OH)₃ [46–48].

The form and dispersion states of Nd₂O₃ in the imide oligomers were further assessed by XRD characterization. Figure 4 shows the XRD patterns of the imide oligomer and Nd₂O₃-modified imide oligomer. In the XRD pattern, a broad amorphous diffraction peak appeared between 10° and 30° in all of the samples, indicating that the imide oligomer substrate was amorphous. This was probably because the molecular chains of the oligomers were irregular, as they were composed of low-weight organic atoms, leading to the formation of amorphous morphological structures. The XRD patterns of the Nd₂O₃ modified oligomer hybrids showed several sharp diffraction peaks centered at approximately 15.9°, 27.7°, 28.7°, 32.1°, 40.3°, 42.9°, 49.6°, 51.3°, and 56.9° when the content of Nd₂O₃ was greater than 0.2 wt%. Moreover, with the increase in the Nd₂O₃ content, the intensity of the relevant crystallization absorption peaks of modified oligomers increased significantly,

which can probably be attributed to the crystallization characteristics of neodymium oxide. These peaks were found to be related to $\text{Nd}(\text{OH})_3$ (ICDD PDF 06-0601) after indexing in the ICDD PDF2 database. The formation of $\text{Nd}(\text{OH})_3$ was due to the hydration of Nd_2O_3 during the imidization reaction [46–48], indicating that Nd_2O_3 was successfully added into the imide oligomer in a specific chemical form. Consequently, the formed $\text{Nd}(\text{OH})_3$ might react with the PI matrix or a byproduct during the subsequent curing process to form a new structure. Additionally, the preparation of modified oligomers with different Nd_2O_3 contents (0.2, 0.4, 0.6, 0.8, and 1 wt%) was used to identify the optimal content of Nd_2O_3 , for which the modified PI would obtain the best thermal oxidation stability.

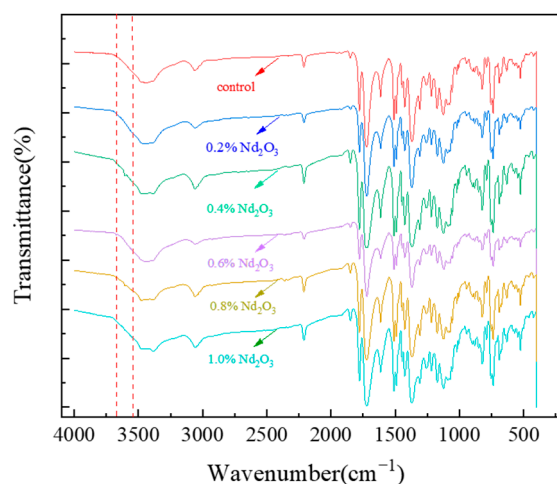


Figure 3. The FTIR spectra of the imide oligomers with different Nd_2O_3 content.

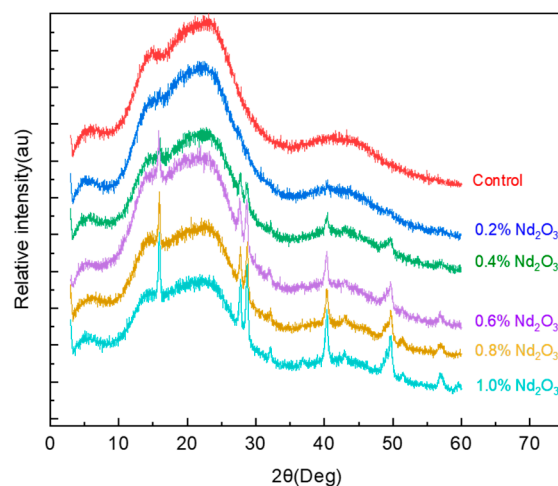


Figure 4. The XRD spectra of the imide oligomers with different Nd_2O_3 contents.

The FTIR and XRD results already demonstrated that Nd_2O_3 changed to the chemical structure of neodymium hydroxide after addition to the imide oligomers. To further demonstrate the physical morphology of neodymium hydroxide in the oligomers, the micro morphologies of the modified imide oligomer powders were observed by SEM, as shown in Figure 5. A comparison of the surface morphology between the pure imide oligomer and 0.8% Nd_2O_3 -modified oligomers revealed no significant differences. The presence of neodymium hydroxide particles could not be directly observed on the surface of the modified oligomers; however, the existence of neodymium elements could be found after energy spectrum analysis. Consequently, we inferred that $\text{Nd}(\text{OH})_3$ was dissolved in the imide oligomers after the imidization reaction.

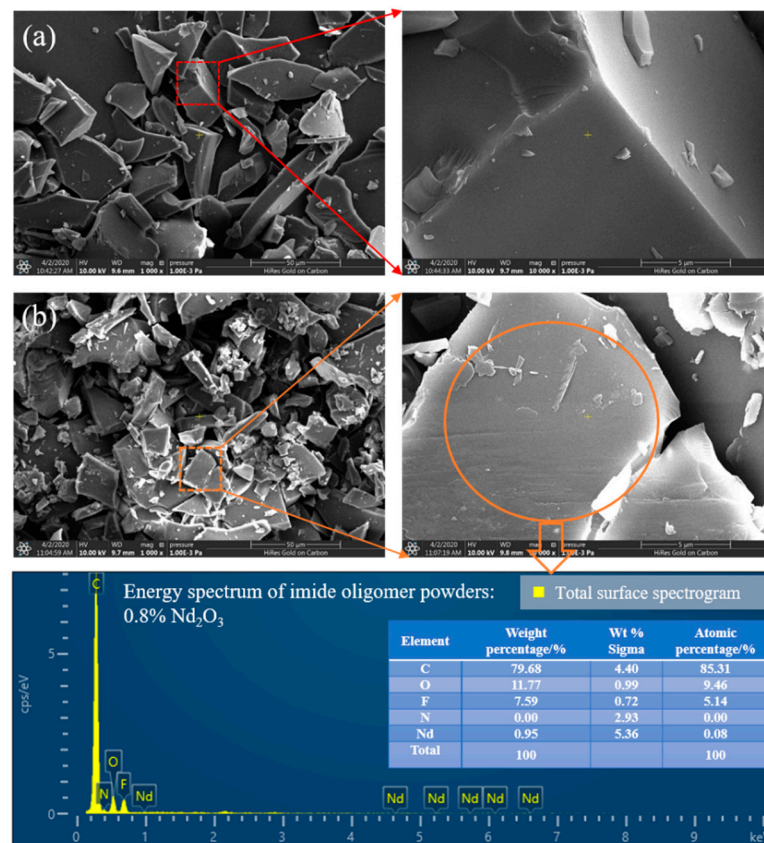


Figure 5. The SEM pattern of the imide oligomer powders: (a) control and (b) 0.8% Nd_2O_3 .

A rheology test was used to study the effect of Nd_2O_3 content on the rheological properties. As shown in Figure 6, the minimum viscosities of the modified oligomers with 0.2, 0.4, 0.6, 0.8, and 1 wt% Nd_2O_3 were 118.6, 119.0, 132.5, 150.7, and 182.6 Pa·s, respectively. We found that the lowest viscosity of the modified oligomers increased gradually and the temperature of the lowest viscosity decreased slowly with increasing Nd_2O_3 content, which contributed to the adsorption of imide oligomers by the nano Nd_2O_3 particles and reduced the motility of the oligomeric molecular chains. The higher the content of neodymium oxide, the more obvious the impact on the rheological properties of the modified oligomers. However, because the mass fraction of Nd_2O_3 was less than 1 wt%, the effect of neodymium oxide on the viscosity would not significantly change the process performance.

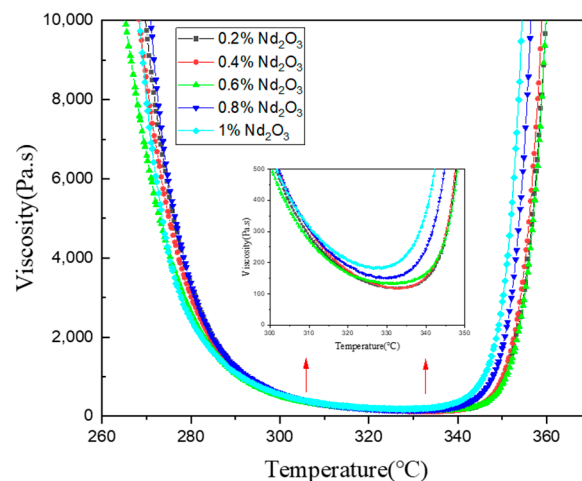


Figure 6. The rheological properties of oligomers with different Nd_2O_3 contents.

3.2. Thermomechanical Properties of Modified Polyimides

The DMA results of the PIs are shown in Figure 7. According to the diagram, after the addition of Nd_2O_3 , the glass transition temperature (T_g) of the PI polymer declined. Moreover, for the modified PI, with increasing Nd_2O_3 content, the T_g value showed an overall downward trend. These results showed evidence that Nd_2O_3 hindered collisions among the reactive crosslinking groups, thus blocking the movement of the oligomers and resulting in the decreased density of cross-linked modified PI ($\text{PI}/\text{Nd}_2\text{O}_3$ hybrid) and reduced T_g . With increasing Nd_2O_3 content, more hindered collisions occurred and the T_g of the $\text{PI}/\text{Nd}_2\text{O}_3$ hybrid declined gradually. However, as the addition of Nd_2O_3 was not more than 1 wt%, the neodymium oxide would not significantly worsen the T_g of the modified polyimide.

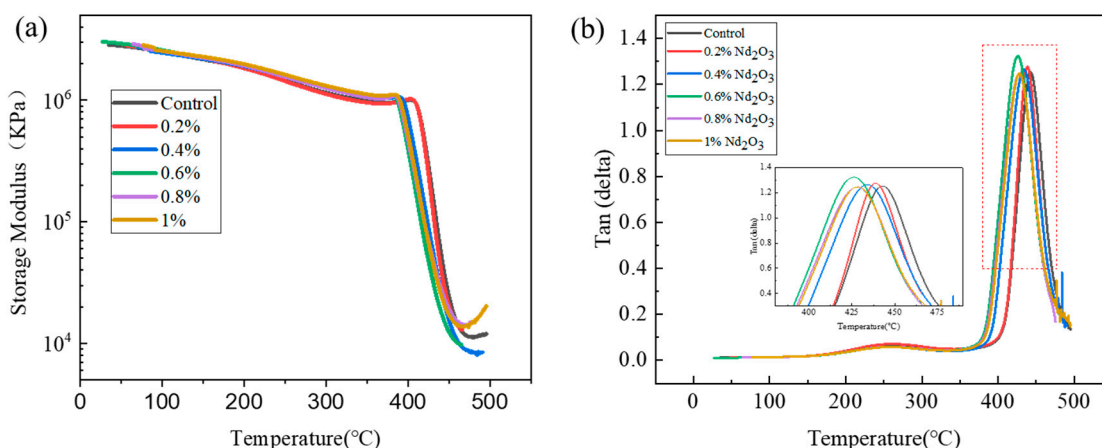


Figure 7. The DMA curve of the polyimide with different contents of Nd_2O_3 : (a) storage modulus and (b) $\tan \delta$.

3.3. Thermal Decomposition Properties of the Modified Polyimides

To study the effect of Nd_2O_3 enhancement on the thermal stability of the $\text{PI}/\text{Nd}_2\text{O}_3$ hybrids, TGA was performed in air in the temperature range of 40–800 °C. The TGA curves of the pure PI and $\text{PI}/\text{Nd}_2\text{O}_3$ hybrids are illustrated in Figure 8. For the thermal stability of the pure PI and $\text{PI}/\text{Nd}_2\text{O}_3$ hybrids, the 5% weight-loss temperature ($T_{d5\%}$) and 10% weight-loss temperature ($T_{d10\%}$) are listed in Table 1. The results revealed that the $\text{PI}/\text{Nd}_2\text{O}_3$ hybrids exhibited a higher decomposition temperature than that of pure PI, and the $T_{d5\%}$ values of these hybrids appeared to improve with an increase in the Nd_2O_3 content. With increased Nd_2O_3 loading from 0 to 0.4 wt%, the $T_{d5\%}$ of the $\text{PI}/\text{Nd}_2\text{O}_3$ hybrids increased from 557 °C to 574 °C, while the $T_{d10\%}$ of the $\text{PI}/\text{Nd}_2\text{O}_3$ hybrids increased from 574 °C to 584 °C. When the Nd_2O_3 loading exceeded 0.4 wt%, the $T_{d5\%}$ and $T_{d10\%}$ improved slowly. This meant that Nd_2O_3 could prevent the thermal oxygen degradation of the PI matrix with low filler content. Meanwhile, the enhanced thermal stability of the $\text{PI}/\text{Nd}_2\text{O}_3$ hybrid would possibly depend on the Nd_2O_3 bonds physically or chemically interacting with the PI matrix. The mechanism was further assessed by XRD.

The weight loss during the heating process was definitely due to the escape of gaseous products, which resulted from the fracture of PI molecule chains. To further investigate the thermal degradation mechanisms of the pure PI and $\text{PI}/\text{Nd}_2\text{O}_3$ hybrids, the release of the degradation products was examined by TGA-FTIR under an air atmosphere at different temperatures. A stacked plot of the FTIR spectra of the byproducts that escaped from TGA during the degradation process is illustrated in Figure 9, and the following characteristic bands were observed during the pyrolysis of PI. The bands in the range of 3500–3800 cm^{-1} were associated with the stretching of O–H and were derived from H_2O ; the peaks at around 2360 and 2322 cm^{-1} were characteristic bands of CO_2 ; the characteristic double bands (2180 and 2110 cm^{-1}) belonged to CO; and the bands at approximately 1152 cm^{-1} were assigned to the symmetric stretching vibrations of F–C–F,

arising from CF_3H , which were only significantly observed when the temperature was above $550\text{ }^\circ\text{C}$ and completely disappeared at $650\text{ }^\circ\text{C}$. These results indicate that the major thermal degraded products were CO_2 , CO , H_2O , and CF_3H . Meanwhile, the CO_2 was the predominant gaseous byproduct throughout the thermal degradation process under the oxygen atmosphere. Additionally, we found that the pure PI and PI/ Nd_2O_3 hybrids had similar volatilized products, except for the temperature at which volatilized products begin to be generated. It was certainly clear that the CO_2 of the PI/ Nd_2O_3 hybrids was observed at $575\text{ }^\circ\text{C}$ (Figure 9b), which was much higher than that of pure PI (Figure 9a). The intensity of volatilized CO_2 peaks increased slowly from $475\text{ }^\circ\text{C}$ to $550\text{ }^\circ\text{C}$, whereas it was found to increase rapidly when the temperature exceeded $550\text{ }^\circ\text{C}$. We concluded that the PI/ Nd_2O_3 hybrids exhibited a significantly better thermal decomposition temperature compared to the pure PI, which corresponded to the TGA results.

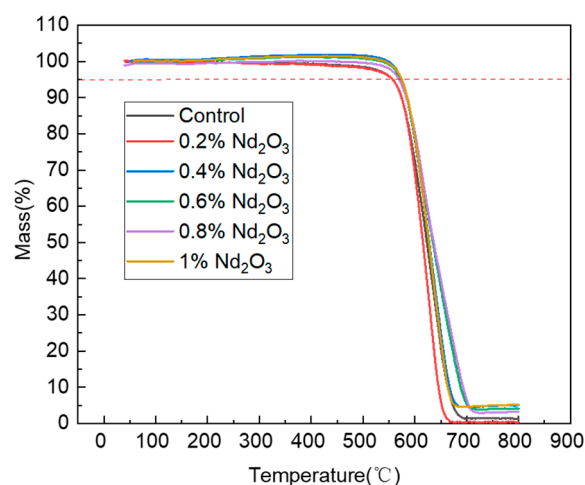


Figure 8. The TGA curves of the polyimides with different Nd_2O_3 contents.

Table 1. The TGA database of the polyimide with different Nd_2O_3 contents ($T_{d5\%}$, $T_{d10\%}$).

Content of Nd_2O_3 /%	$T_{d5\%}$ (Air)/ $^\circ\text{C}$	$T_{d10\%}$ (Air)/ $^\circ\text{C}$
0	557	574
0.2	557	574
0.4	574	584
0.6	573	584
0.8	570	584
1.0	575	585

3.4. Thermal Oxidative Stability of the Modified Polyimides

To better study the thermal oxidative stability of the Nd_2O_3 -modified PIs in a long-term service environment, the weight loss changes of the pure PI and PI/ Nd_2O_3 hybrids were evaluated by an isothermal thermo-oxygen aging method. The weight loss rates of the modified PIs with different Nd_2O_3 contents during isothermal aging at $350\text{ }^\circ\text{C}$ for 450 h are shown in Figure 10. The weight loss rates of both the PI/ Nd_2O_3 hybrids and pure PI increased with prolonged aging time. However, the weight loss rates of the PI/ Nd_2O_3 hybrids were notably lower than that of the pure PI. When the aging time was 450 h, the weight loss rates of the PI/ Nd_2O_3 hybrids at 0, 0.2, 0.4, 0.6, 0.8, and 1 wt% were 10.25, 8.84, 7.11, 7.23, 7.04, and 7.29%, respectively. Thus, the weight loss rates of the 0.2, 0.4, 0.6, 0.8, and 1 wt% samples decreased by 13.8, 30.6, 29.5, 31.3, and 28.9%, respectively, compared to the pure PI. We concluded that the thermal-oxidative stability of the modified PIs was

dramatically better than that of the pure PIs when the Nd_2O_3 content was between 0.4 wt% and 1 wt%, which was similar to the TGA results.

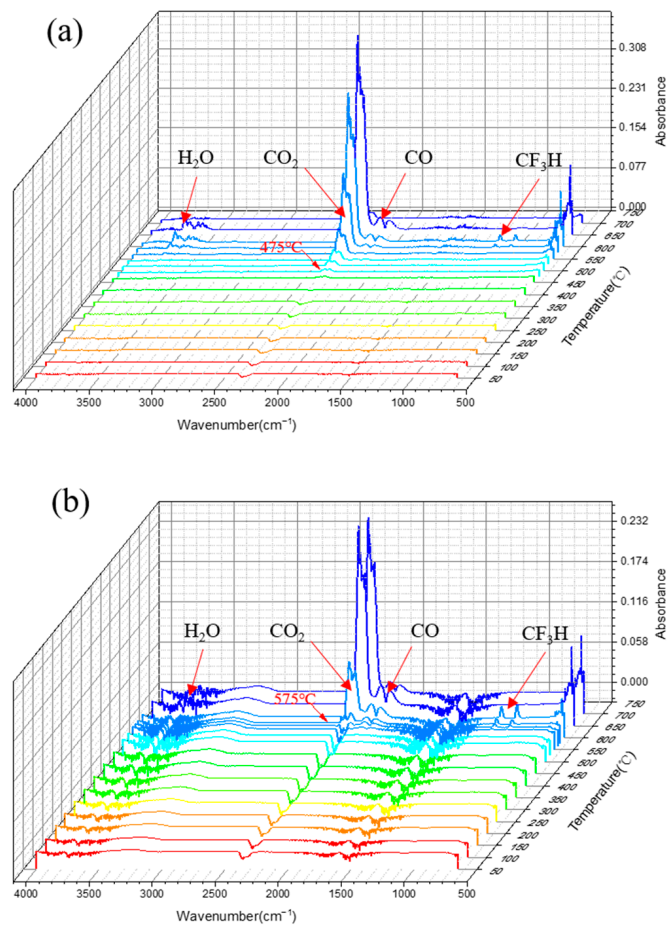


Figure 9. The release of degradation products was examined by TGA-FTIR at different temperatures: (a) control and (b) 0.4% Nd_2O_3 .

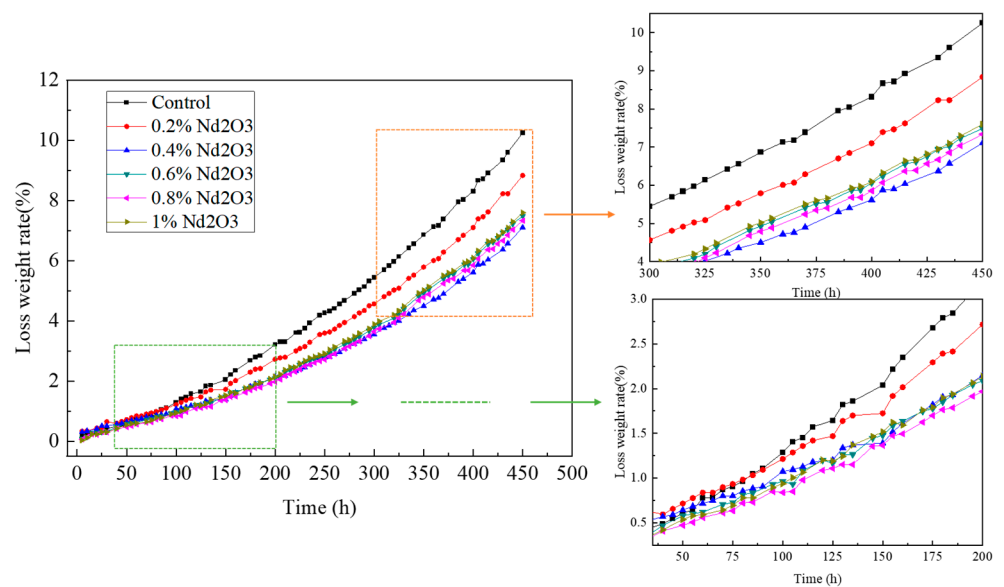


Figure 10. The weight loss rate of the polyimide with different contents of Nd_2O_3 at 350 $^{\circ}\text{C}$.

As shown in Figure 11, the surface morphologies of the modified PI resin with different Nd_2O_3 contents (0, 0.2%, 0.4%, 0.6%, 0.8%, and 1%) after isothermal aging at 350 °C for 450 h were characterized by SEM. We found that after prolonged high temperature aging, numerous pores were generated on the surface of the unmodified PI resin. The structure and size of the pores were randomly distributed, and the density of the pores was high. The pores presented a semi-continuous state. However, the surface porosity of the Nd_2O_3 -modified PI resin was significantly reduced, and the pore size was slightly larger than that of the unmodified PI, while the density of the pores was significantly reduced. Conversely, the internal structure (Figure 12) of the PI and modified PIs was at a distance away from the aerobic area of the surface, while the intact microstructure and accumulation density were still maintained, and the pores caused by resin decomposition were not observed. Additionally, the enhancement of the thermal-oxidation stability was due to the formation of $\text{Nd}_2\text{O}_3/\text{PI}$ hybrids, which could inhibit the diffusion of oxygen and reduce the degradation of the PI resin.

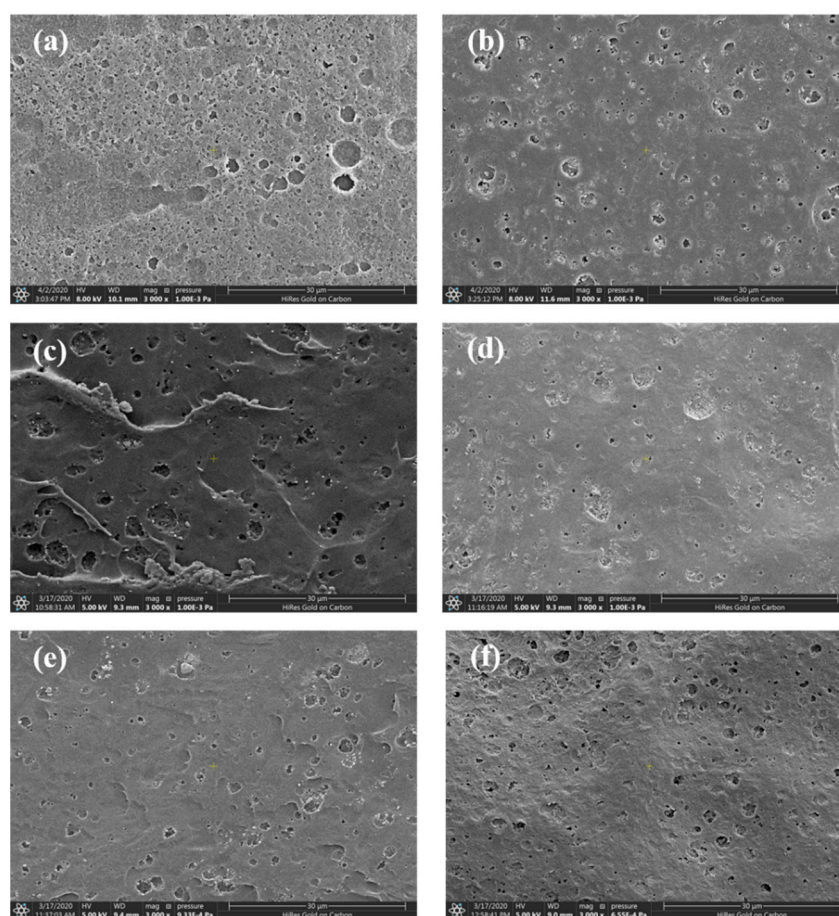


Figure 11. The SEM patterns of the resin surface after isothermal aging at 350 °C for 450 h: (a) control; (b) 0.2 wt% Nd_2O_3 , (c) 0.4 wt% Nd_2O_3 , (d) 0.6 wt% Nd_2O_3 , (e) 0.8 wt%, and (f) 1 wt% Nd_2O_3 .

For the enhancement mechanism of thermal-oxidation stability, XRD analysis was carried out on the pure PI and Nd_2O_3 -modified imide oligomer (0.8 wt%), while the $\text{Nd}_2\text{O}_3/\text{PI}$ hybrids (0.8 wt%) were used to investigate the interactions between Nd_2O_3 and PI, as shown in Figure 13. A broad amorphous diffraction peak between 10° and 30° was found from the XRD patterns of the cured, pure PI, showing its amorphous structure. The characteristic diffraction peak of $\text{Nd}(\text{OH})_3$ was found in the modified imide oligomer (0.8 wt%), which meant that the Nd_2O_3 was converted into $\text{Nd}(\text{OH})_3$. The XRD patterns of the $\text{Nd}_2\text{O}_3/\text{PI}$ hybrids (0.8 wt%) were almost the same as that of pure PI. The disappearance of the characteristic diffraction peak for $\text{Nd}(\text{OH})_3$ obviously

demonstrated that $\text{Nd}(\text{OH})_3$ was chemically incorporated into the PI resin matrix and formed the $\text{Nd}_2\text{O}_3/\text{PI}$ hybrids. This was certainly attributed to the reactivity of the hydroxyl group in $\text{Nd}(\text{OH})_3$, which led to an increase in the interactions between the Nd_2O_3 and PI matrix during the curing process. The formation of $\text{Nd}_2\text{O}_3/\text{PI}$ hybrids could inhibit the diffusion of oxygen molecules in the crosslinked PI resin structure, which was attributed to strong interaction between the neodymium oxide and the polyimide matrix during the curing process. Consequently, this slowed down the reaction activity of the oxygen molecules, thus hindering the fracture of the crosslinked chains caused by thermal oxygen decomposition, resulting in the enhancement of the thermal-oxidation stability of PI [47,48].

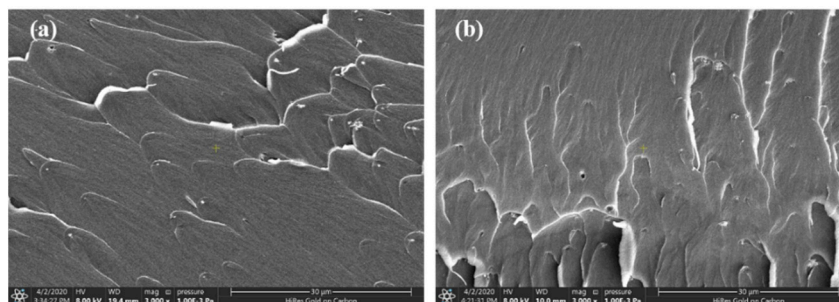


Figure 12. The SEM patterns of the resin section after isothermal aging at 350 °C for 450 h: (a) control and (b) 0.8 wt% Nd_2O_3 .

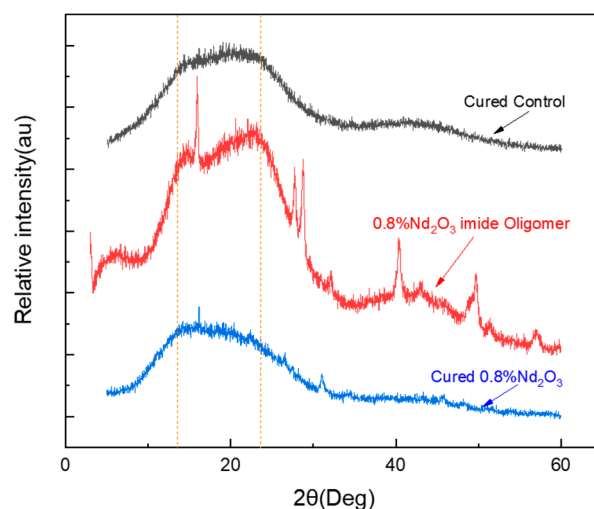


Figure 13. The XRD spectra of the $\text{Nd}_2\text{O}_3/\text{PI}$ hybrids (0.8 wt%) compared to the modified imide oligomer.

4. Conclusions

The phenylethynyl terminated PIs modified with various Nd_2O_3 contents were successfully prepared by high-speed stirring and ultrasonic dispersion methods, and the thermal-oxidation stability of the pure PI and modified PIs ($\text{PI}/\text{Nd}_2\text{O}_3$ hybrids) was evaluated by TGA-IR and the isothermal thermo-oxygen aging methods. The TGA results indicate that the $T_{d5\%}$ of the $\text{PI}/\text{Nd}_2\text{O}_3$ hybrids improved from 557 °C to 575 °C when the added amount of Nd_2O_3 in the modified PIs was between 0.4 wt% and 1 wt%. Meanwhile, the evolved gas was analyzed by TGA-IR, which showed that CO_2 was the dominant degradation product. Furthermore, the weight loss rate of the $\text{PI}/\text{Nd}_2\text{O}_3$ hybrids was significantly reduced by 28% to 31% after isothermal thermo-oxygen aging at 350 °C for 450 h compared to that of pure PI, when the content of Nd_2O_3 was between 0.4 wt% and 1 wt%. This corresponded to the TGA results and indicated a dramatically higher thermal oxidation stability. The outstanding thermo-oxidative stability was attributed to the chemi-

cal incorporation of Nd₂O₃ into the PI matrix, which could inhibit oxygen diffusion and slow down PI resin degradation due to the characteristics of the Nd elements.

Author Contributions: Conceptualization, P.Z., J.B., Y.Z. and X.C.; Methodology, P.Z. and H.L.; Validation, P.Z. and J.B.; Formal analysis, P.Z. and J.B.; Investigation, P.Z., H.L., Y.Y., T.Y., J.S. and X.Z.; Resources, P.Z.; Data curation, P.Z.; Writing—original draft preparation, P.Z.; Writing—review and editing, P.Z., J.B., Y.Z. and X.C.; Supervision, J.B., Y.Z. and X.C.; Project administration, J.B., Y.Z. and X.C.; Funding acquisition, J.B., Y.Z. and X.C. All authors have read and agreed to the published version of the manuscript.

Funding: This research was funded by the National Science and Technology Major Project (2017-VII-0011-0106).

Institutional Review Board Statement: Not applicable.

Informed Consent Statement: Not applicable.

Data Availability Statement: The data presented in this study are available upon request from the corresponding author. The data are not publicly available due to the fact that they are also part of an ongoing study.

Conflicts of Interest: The authors declare no conflict of interest, and the funders had no role in the design of the study; in the writing of the manuscript; or in the decision to publish the results, the collection, analyses, or interpretation of data.

References

1. Liaw, D.J.; Wang, K.L.; Huang, Y.C.; Lee, K.R.; Lai, J.Y.; Ha, C.S. Advanced polyimide materials: Syntheses, physical properties and applications. *Prog. Polym. Sci.* **2012**, *37*, 907–974. [[CrossRef](#)]
2. Liu, H.; Zhao, Y.; Li, N.; Li, S.; Li, X.; Liu, Z.; Cheng, S.; Wang, K.; Du, S. Effect of polyetherimide sizing on surface properties of carbon fiber and interfacial strength of carbon fiber/polyetheretherketone composites. *Polym. Compos.* **2021**, *42*, 931–943. [[CrossRef](#)]
3. Çakir, M.; Akin, E. Characterization of carbon fiber-reinforced thermoplastic and thermosetting polyimide matrix composites manufactured by using various synthesized PI precursor resins. *Compos. Part B Eng.* **2022**, *231*, 109559. [[CrossRef](#)]
4. Sun, J.; Han, Y.; Zhao, Z.; Wang, G.; Zhan, S.; Ding, J.; Liu, X.; Guo, Y.; Zhou, H.; Zhao, T. Improved toughness of phthalonitrile composites through synergistic toughening methods. *Compos. Commun.* **2021**, *26*, 100779. [[CrossRef](#)]
5. Alston, W.B.; Scheiman, D.A.; Sivko, G.S. A comparison study: The new extended shelf life isopropyl ester PMR technology versus the traditional methyl ester PMR approach. *J. Appl. Polym. Sci.* **2010**, *99*, 3549–3564. [[CrossRef](#)]
6. Hasegawa, M.; Nomura, R. Thermal-and solution-processable polyimides based on mellophanic dianhydride and their applications as heat-resistant adhesives for copper-clad laminates. *React. Funct. Polym.* **2011**, *71*, 109–120. [[CrossRef](#)]
7. Çakir, M.; Akin, E. Mechanical properties of low-density heat-resistant polyimide-based advanced composite sandwich panels. *Polym. Compos.* **2022**, *43*, 827–847. [[CrossRef](#)]
8. Wang, J.; Yi, X.S. Preparation and the properties of PMR-type polyimide composites with aluminum nitride. *J. Appl. Polym. Sci.* **2010**, *89*, 3913–3917. [[CrossRef](#)]
9. Hergenrother, P.M.; Smith, J.G., Jr. Chemistry and properties of imide oligomers end-capped with phenylethynylphthalic anhydrides. *Polymer* **1994**, *35*, 4857–4864. [[CrossRef](#)]
10. Bryant, R.G.; Jensen, B.J.; Hergenrother, P.M. Chemistry and properties of a phenylethynyl-terminated polyimide. *J. Appl. Polym. Sci.* **1996**, *59*, 1249–1254. [[CrossRef](#)]
11. Yamaguchi, H.; Aoki, F. Properties of Asymmetric BPDA based phenylethynyl terminated thermosetting polyimide and its composite. *J. Photopolym. Sci. Technol.* **2006**, *19*, 269–272. [[CrossRef](#)]
12. Yu, P.; Wang, Y.; Yu, J.R.; Zhu, J.; Hu, Z. Synthesis and characterization of phenylethynyl-terminated polyimide oligomers derived from 2,3,3',4'-diphenyl ether tetracarboxylic acid dianhydride and 3,4'-oxydianiline. *Chin. J. Polym. Sci.* **2016**, *34*, 122–134. [[CrossRef](#)]
13. Xu, X.; Liu, Y.; Lan, B.; Mo, S.; Zhai, L.; He, M.; Fan, L. High Thermally Stable and Melt Processable Polyimide Resins Based on Phenylethynyl-Terminated Oligoimides Containing Siloxane Structure. *Materials* **2020**, *13*, 3742. [[CrossRef](#)] [[PubMed](#)]
14. Yu, P.; Wang, Y.; Yu, J.R.; Zhu, J.; Hu, Z. Phenylethynyl-terminated polyimide oligomers with low viscosity and good thermal properties. *Mater. Sci. Forum.* **2016**, *848*, 167–173. [[CrossRef](#)]
15. Xiao, T.J.; Gao, S.Q.; Hu, A.J.; Wang, X.C.; Yang, S.Y. Thermosetting polyimides with improved impact toughness and excellent thermal and thermo-oxidative stability. *High Perform. Polym.* **2001**, *13*, 287–300. [[CrossRef](#)]
16. Shi, Z.; Hasegawa, M.; Shindo, Y.; Yokata, R.; He, F.; Yamaguchi, H.; Ozawa, H. Thermo-processable polyimides with high thermo-oxidative stability as derived from oxydiphthalic anhydride and bisphenol A type dianhydride. *High Perform. Polym.* **2000**, *12*, 377–394. [[CrossRef](#)]

17. Torrecillas, R.; Baudry, A.; Dufay, J.; Mortaigne, B. Thermal degradation of high performance polymers-influence of structure on polyimide thermostability. *Polym. Degrad. Stab.* **1996**, *54*, 267–274. [[CrossRef](#)]
18. Serafini, T.T.; Delvigs, P.; Lightsey, G.R. Thermally stable polyimides from solutions of monomeric reactants. *J. Appl. Polym. Sci.* **1972**, *16*, 905–915. [[CrossRef](#)]
19. Hou, T.H.; Wilkinson, S.P.; Johnston, N.J.; Pater, R.H.; Schneider, T. Processing and properties of IM7/LARC™-RP46 polyimide composites. *High Perform. Polym.* **1996**, *8*, 491–505. [[CrossRef](#)]
20. Chuang, K.C.; Bowles, K.J.; Papadopoulos, D.S.; DeNise, H.G.; Linda, M.G. A high Tg PMR polyimide composites (DMBZ-15). *J. Adv. Mater.* **2001**, *33*, 33–38.
21. Connell, J.W.; Smith, J.J.; Hergenrother, P.M.; Criss, J.M. High Temperature Transfer Molding Resins: Laminate Properties of PETI-298 and PETI-330. *High Perform. Polym.* **2003**, *15*, 375–394. [[CrossRef](#)]
22. Connell, J.W.; Smith, J.J.; Hergenrother, P.M. Criss High Temperature Transfer Molding Resin: Preliminary Composite Properties of PETI-375. *Int. SAMPE Symp. Exhi.* **2004**, *5*, 16–20.
23. Whitley, K.S.; Collins, T.J. Mechanical Properties of T650-35/AFR-PE-4 at Elevated Temperatures for Lightweight Aeroshell Designs. In Proceedings of the 47th AIAA/ASME/ASCE/AHS/ASC SDM Conference, Newport, RI, USA, 1–4 May 2006; pp. 2006–2202.
24. Ogasawara, T.; Takashi, I.; Yokota, R.; Ozawa, H.; Taguchi, M.; Sato, R.; Shigenari, Y.; Miyagawa, K. Processing and properties of carbon fiber reinforced triple-A Polyimide (Tri-A PI) matrix composites. *Adv. Compos. Mater.* **2003**, *11*, 277–286. [[CrossRef](#)]
25. Yu, P.; Wang, Y.; Yu, J.; Zhu, J.; Hu, Z. Influence of different ratios of a-ODPA/a-BPDA on the properties of phenylethynyl terminated polyimide. *J. Polym. Res.* **2018**, *25*, 110. [[CrossRef](#)]
26. Ogasawara, T.; Ishida, Y.; Ishikawa, T.; Yokota, R. Characterization of multi-walled carbon nanotube/phenylethynyl terminated polyimide composites. *Compos. Part A Appl. Sci. Manuf.* **2004**, *35*, 67–74. [[CrossRef](#)]
27. Lebrón-Colón, M.; Meador, M.A.; Gaier, J.R.; Solá, F.; McCorkle, L.S. Reinforced thermoplastic polyimide with dispersed functionalized single wall carbon nanotubes. *ACS Appl. Mater. Interfaces* **2010**, *2*, 669–676. [[CrossRef](#)]
28. Chou, W.J.; Wang, C.C.; Chen, C.Y. Thermal behaviors of polyimide with plasma-modified carbon nanotubes. *Polym. Degrad. Stab.* **2008**, *93*, 745–752. [[CrossRef](#)]
29. Huang, Z.; Wang, S.; Li, H.; Zhang, S.; Tan, Z. Thermal stability of several polyaniline/rare earth oxide composites. *J. Therm. Anal. Calorim.* **2014**, *115*, 259. [[CrossRef](#)]
30. Babanzadeh, S.; Mehdipour-Ataei, S.; Mahjoub, A.R. Effect of nanosilica on the dielectric properties and thermal stability of polyimide/SiO₂ nanohybrid. *Des. Monomers Polym.* **2013**, *16*, 417–424. [[CrossRef](#)]
31. Nikolaeva, A.L.; Gofman, I.V.; Yakimansky, A.V.; Ivan'kova, E.M.; Gulii, N.S.; Teplonogova, M.A.; Ivanova, O.S.; Baranchikov, A.E.; Ivanov, V.K. Interplay of polymer matrix and nanosized Redox dopant with regard to thermo-oxidative and pyrolytic stability: CeO₂ nanoparticles in a milieu of aromatic polyimides. *Mater. Today Commun.* **2020**, *22*, 100803. [[CrossRef](#)]
32. Liu, Z.; Fan, J.; Feng, J.; Li, M.; Hu, Y.; Hao, W.; Feng, F. Study on the use of rare earth stabilizer as poly (vinyl chloride) stabilizer. *J. Vinyl Addit. Technol.* **2020**, *26*, 536–547. [[CrossRef](#)]
33. Hu, Y.; Zhan, W.; Wu, Z.; Tang, Y.; Huang, Y.; Ding, X.T.; Chen, D. Poly (styrene-alt-maleic anhydride) ionic salt functionalized reduced graphene oxide doped with rare earth ions for anti-corrosion performance enhancement. *J. Appl. Polym. Sci.* **2021**, *138*, 50666. [[CrossRef](#)]
34. Xiao, W.; Li, X.; Guo, H.; Wang, Z.; Yang, B.; Wu, X. Preparation and properties of composite polymer electrolyte modified with nano-size rare earth oxide. *J. Cent. South Univ.* **2012**, *19*, 3378–3384. [[CrossRef](#)]
35. Phani, K.K.; Niyogi, S.K. Elastic modulus-porosity relation in polycrystalline rare-earth oxides. *J. Am. Ceram. Soc.* **1987**, *70*, 362–366. [[CrossRef](#)]
36. Dong, B.; Cao, B.; He, Y.; Liu, Z.; Li, Z.; Feng, Z. Temperature sensing and in vivo imaging by molybdenum sensitized visible upconversion luminescence of rare-earth oxides. *Adv. Mater.* **2012**, *24*, 1987–1993. [[CrossRef](#)]
37. Wang, S.; Huang, Z.; Wang, J.; Li, Y.; Tan, Z. Thermal stability of several polyaniline/rare earth oxide composites (I): Polyaniline/CeO₂ composites. *J. Therm. Anal. Calorim.* **2012**, *107*, 1199–1203. [[CrossRef](#)]
38. Feng, C.; Liang, M.; Zhang, Y.; Jiang, J.; Huang, J.; Liu, H. Synergism effect of CeO₂ on the flame retardant performance of intumescent flame retardant polypropylene composites and its mechanism. *J. Anal. Appl. Pyrolysis* **2016**, *122*, 405–414. [[CrossRef](#)]
39. Feng, C.; Zhang, Y.; Liu, S.; Chi, Z.; Xu, J. Synergistic effect of La₂O₃ on the flame retardant properties and the degradation mechanism of a novel PP/IFR system. *Polym. Degrad. Stab.* **2012**, *97*, 707–714. [[CrossRef](#)]
40. Zhang, M.; Wang, X.; Liu, W. Tribological behavior of LaF₃ nanoparticles as additives in poly-alpha-olefin. *Ind. Lubr. Tribol.* **2013**, *65*, 226–235. [[CrossRef](#)]
41. Wang, H.; Feng, X.; Shi, Y.; Lu, X. A study on the tribological properties of self-assembled method treated nano-La₂O₃ filled PTFE/PEEK composites. *J. Reinf. Plast. Compos.* **2009**, *28*, 645–655. [[CrossRef](#)]
42. Li, H.; Wang, S.X.; Huang, Z.; Zhang, S.; Li, Y.; Han, L.; Tan, Z. Effect Nd₂O₃ content on electrochemical performance of polyaniline/Nd₂O₃ composites. *Polym. Adv. Technol.* **2014**, *25*, 1163–1168. [[CrossRef](#)]
43. Sato, S.; Takahashi, R.; Kobune, M.; Gotoh, H. Basic properties of rare earth oxides. *Appl. Catal. A* **2009**, *356*, 57–63. [[CrossRef](#)]
44. Bian, L.J.; Qian, X.F.; Yin, J.; Lu, Q.H.; Liu, L.; Zhu, Z.K. Preparation and properties of rare earth oxide/polyimide hybrids. *Polym. Test.* **2002**, *21*, 841–845. [[CrossRef](#)]

45. Falcao, E.A.; Aguiar, L.W.; Guo, R.; Bhalla, A.S. Optical absorption of Nd₂O₃-Doped polyvinylidene fluoride films. *Mater. Chem. Phys.* **2021**, *258*, 123904. [[CrossRef](#)]
46. Nagao, M.; Hamano, H.; Hirata, K.; Kumashiro, R.; Kuroda, Y. Hydration process of rare-earth sesquioxides having different crystal structures. *Langmuir* **2003**, *19*, 9201. [[CrossRef](#)]
47. Zhang, P.; Bao, J.; Jiang, Z.; Dong, B.; Chen, X. Enhancing thermo-oxidative stability of thermoset polyimide composites using nano neodymium oxide particles. *J. Mater. Res. Technol.* **2021**, *14*, 2638–2649. [[CrossRef](#)]
48. Hamano, H.; Kuroda, Y.; Yoshikawa, Y.; Nagao, M. Adsorption of water on Nd₂O₃: Protecting a Nd₂O₃ sample from hydration through surface fluoridation. *Langmuir* **2000**, *16*, 6961. [[CrossRef](#)]